SANDIA REPORT SAND81-2083 • Unlimited Release • UC-62e
Printed December 1981

Contact Stresses on a Thin Plate After Large Displacements to a Full Parabolic Surface

Robert C. Reuter, Jr., Rodney K. Wilson

Prepared by
Sandia National Laboratories
Albuquerque, New Mexico 87185 and Livermore, California 94550
for the United States Department of Energy
under Contract DE-AC04-76DP00789

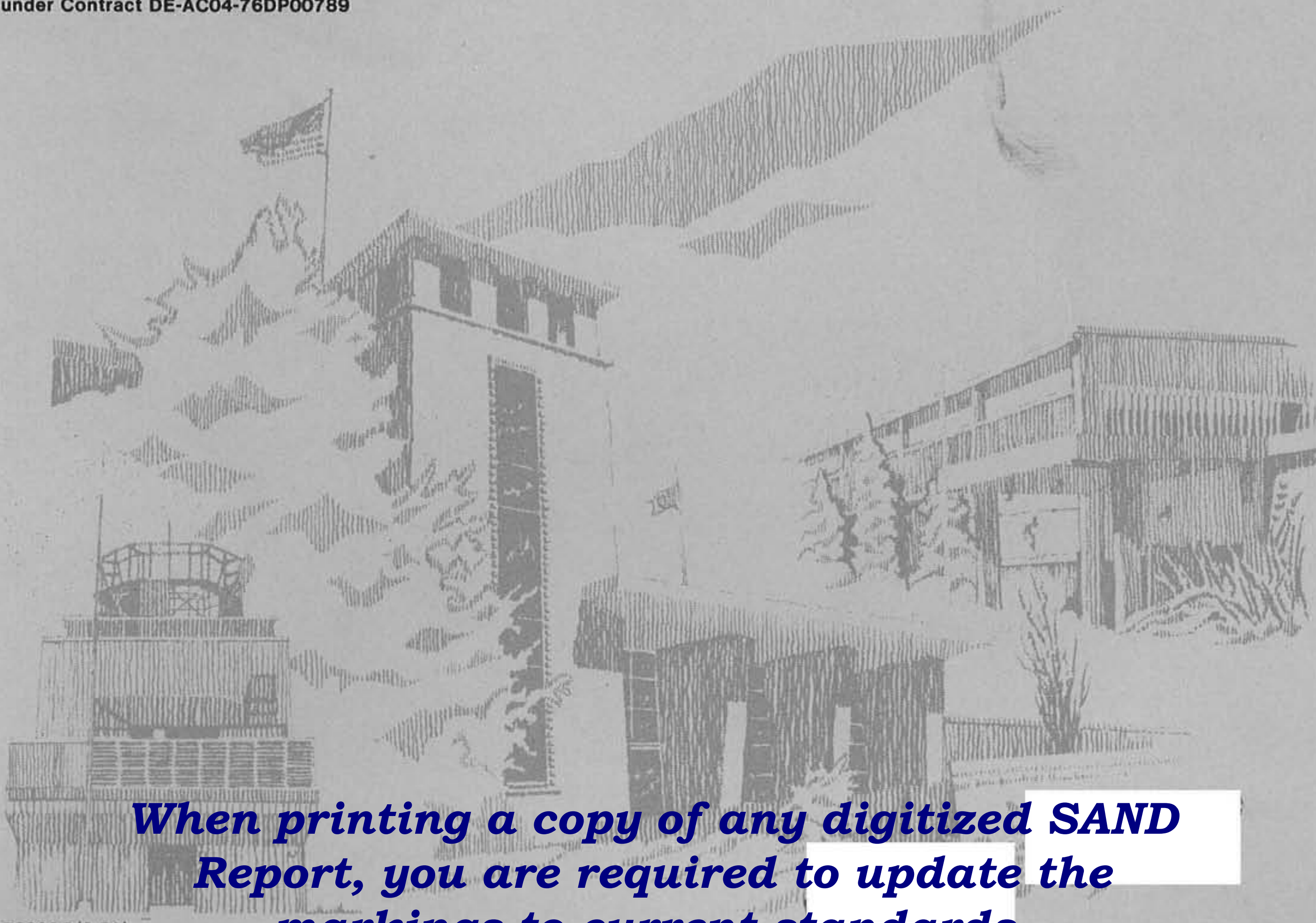

SF2900Q(8-81)

Issued by Sandia National Laboratories, operated for the United States Department of Energy by Sandia Corporation.

Printed in the United States of America
Available from
National Technical Information Service
U.S. Department of Commerce
5285 Port Royal Road
Springfield, VA 22161

NTIS price codes
Printed copy: $6.00
Microfiche copy: A01

SAND81-2083

CONTACT STRESSES ON A THIN PLATE AFTER LARGE DISPLACEMENTS TO A FULL PARABOLIC SURFACE*

Robert C. Reuter, Jr.
Rodney K. Wilson
Sandia National Laboratories
Albuquerque, NM 87185

ABSTRACT

A solution is obtained for the determination of all loads necessary to hold an initially flat, thin, elastic plate in the shape of a prescribed parabolic surface, following large displacement. These loads include spatially varying normal tractions distributed over the back surface of the plate, and a uniform shear force and bending moment applied along the opposing edges which become the rims of the parabola after deformation. The plate represents a reflective surface which is mechanically deformed to the shape of, and bonded to a rigid, parabolic substructure to create a solar collector. After assembly, the normal stresses are those developed in the adhesive which bonds the reflective surface to the substructure. The absence of edge loads along the rims of an actual, formed reflective surface gives rise to local displacement and stress variations (edge effects) which are obtained through a separate solution. Numerical results for the normal stress distribution, local variations and loss of optical quality in the edge effect zone are included.

*This work performed at Sandia National Laboratories supported by the U.S. Department of Energy under contract number DE-AC04-76DP00789.

TABLE OF CONTENTS

ILLUSTRATIONS

NOMENCLATURE

D	flexural rigidity of reflective surface
E	Young's modulus
f	focal length of parabola
h	thickness of reflective panel
k	stiffness of adhesive plus substructure
$M(x)$	bending moment at x
$dM_p(\xi)$	incremental bending moment at ξ
M_R	bending moment applied at rim to maintain true parabolic shape
M_V	moment reaction at vertex
N_V	membrane reaction at vertex
P_C	contact pressure applied over back surface of reflective panel to maintain true parabolic shape
Q_R	Shear force applied at rim to maintain true parabolic shape
s	curvalinear coordinate (arc length) measured along parabola from vertex
$w_R(x)$	displacement of reflective surface at x
x,y	rectangular coordinates
β	panel-adhesive-substructure stiffness parameter
δ_2	second cross-over distance
ζ	coordinate distance measured from rim
η	dimensionless coordinate measured from vertex
ν	Poisson's ratio
ξ	dummy variable
$\sigma_C(x)$	contact stress at x due to forming
$\sigma_R(x)$	contact stress at x due to edge effect
$\phi(x)$	slope of parabola at x
Ψ	dimensionless contact pressure

INTRODUCTION

Line focusing solar collectors in the form of parabolic troughs are often assembled by elastically deforming an initially flat reflective surface to the shape of a premanufactured, parabolic support structure. The reflective surfaces may be thin, mirrored glass panels, mirror laminates, polished metallic panels or panels with various reflective coatings, and are bonded to the parabolic support structure by various choices of adhesives. Figure 1 shows an example of a thin, flat, mirrored panel of strengthened glass elastically deformed and bonded to a prefabricated, sheet metal rib and panel support structure. To offset the tendency of the reflective surface to return to its initially flat state, contact stresses develop in the adhesive beneath it.

A thin, flat panel can be deformed to a parabolic surface by a spatially nonuniform pressure distributed over its surface and a constant bending moment and shear force along each rim of the resulting parabolic surface, as determined herein. The rim loads are necessary from an analytical standpoint to maintain equilibrium and the true parabolic shape locally. When only contact adhesives are used to hold the reflective surface in place, as is frequently done, there is no rim moment or shear applied. These loads are replaced by relatively large, local contact stress variations which develop near the edge to offset the tendency of the reflective surface to achieve zero curvature (a consequence of having no rim moment). Because the true parabolic shape is lost in this region, optical quality of the collector is compromised. This is referred to as the edge effect.

The principal objective of this study is to predict the magnitude, direction and distribution of contact stresses required to hold the reflective surface to the parabolic substructure, taking into account the edge effect. The problem is solved in two phases. First, the pressure distribution required to elastically deform the flat reflective surface panel through large displacements to the true parabolic shape

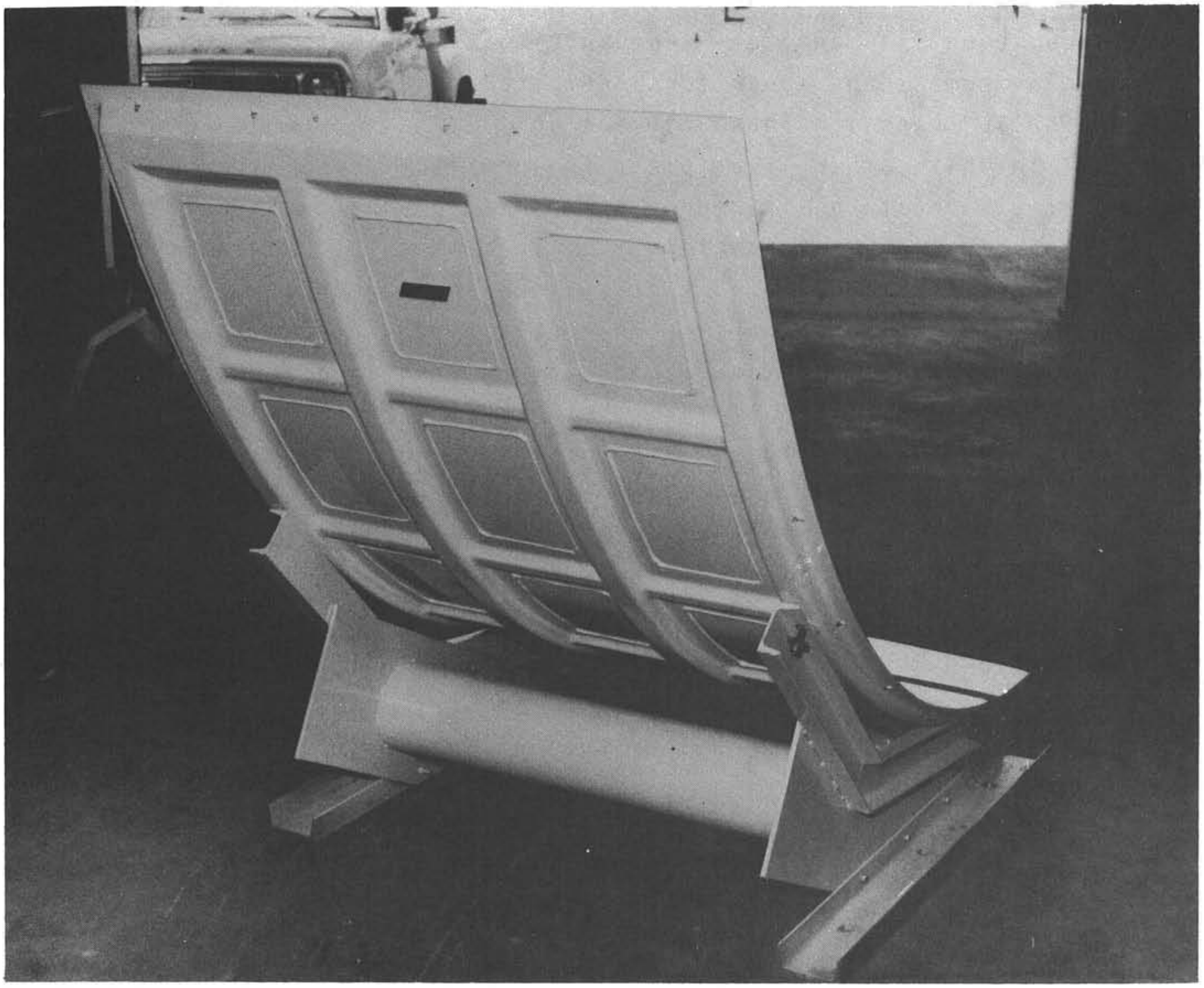

FIGURE 1. Assembled, parabolic, line focusing solar collector

is obtained. The rim moment and shear force are necessarily retained in this phase of the analysis. By changing the sense of these forming pressures, and assuming that spring-back effects are negligible, the corresponding contact stresses are obtained. In the second phase, a rim bending moment and shear force, equal in magnitude and opposite in sense to the rim bending moment and shear force required to achieve the true parabolic shape (in phase 1), are applied to the edge of a semi-infinite, thin, flat plate (the reflective surface) on an elastic foundation (the adhesive layer and substructure). This approach permits calculation of contact stresses between the plate and its foundation, thereby modeling the edge effect. Presumably the true shape of the reflective surface is achieved during mechanical forming, prior to releasing the forming loads. Superposition of the solutions from the two phases gives the desired result, with the free edge condition satisfied. Several conclusions are drawn regarding the dependence of contact stresses and optical quality upon general adhesive and substructure properties.

DEFORMATION TO THE TRUE PARABOLA - THE FORMING PROBLEM

An end view of one half of the reflective surface, after deformation to the parabolic cylinder, is shown in Fig. 2. It is symmetric with respect to the y - z (focal) plane. External loads necessary to achieve the true parabolic shape described by

$$y = \frac{x^2}{4f} \tag{1}$$

are $P_C(x)$, the contact pressure, M_R, the rim bending moment, and Q_R, the rim shear force, hereafter referred to as the residual moment and residual shear. The membrane force, N_V, and the bending moment, M_V, are internal reactions which occur at the vertex of the parabola.

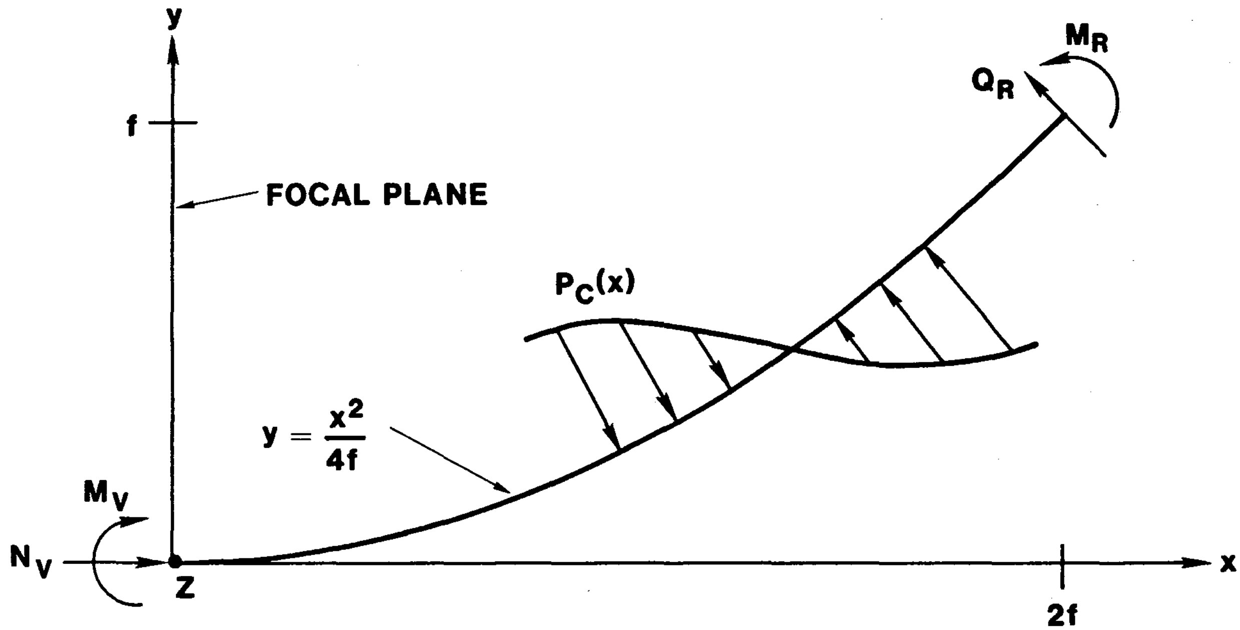

FIGURE 2. Diagram of half of the deformed, reflective surface explicating coordinates, rim loads, vertex reactions and the pressure distribution required to achieve the true parabolic shape.

In his theory for the elastic bending of thin rods by large deformation, see [1] for example, Euler established that the curvature is proportional to the bending moment at any point in the rod. To extend this useful result to the inextensional theory of thin plates it is necessary to require that anticlastic effects be confined to a very small region along edges perpendicular to generators of the deformed plate. Then, the remainder of the plate behaves as though it were experiencing cylindrical bending. This occurs whenever the square of the plate width is large in comparison to the product of the plate thickness and radius of curvature, a condition easily satisfied by geometries in the present investigation. These concepts are covered in [2,3]. Euler's relation can be expressed as

$$D \frac{d\phi(x)}{ds} = M(x) \quad , \tag{2}$$

where D is the flexural rigidity of a plate of thickness, h, material modulus, E, and Poisson's ratio, ν, and is given by

$$D = \frac{Eh^3}{12(1-\nu^2)} \quad .$$

Refering to Fig. 3, s is the curvilinear coordinate along the parabola, and ϕ is the angle formed between a tangent to the parabola and the ξ-axis. Therefore, $(d\phi/ds)$ is the curvature at any point s. Curvature is expressed in rectangular coordinates [5]

$$\frac{d\phi}{ds} = \frac{\dfrac{d^2y}{dx^2}}{\left[1 + \left(\dfrac{dy}{dx}\right)^2\right]^{3/2}} \tag{3}$$

Since the parabolic trough collectors of interest have an aperture equal to 4f, the displacements of a flat panel to the

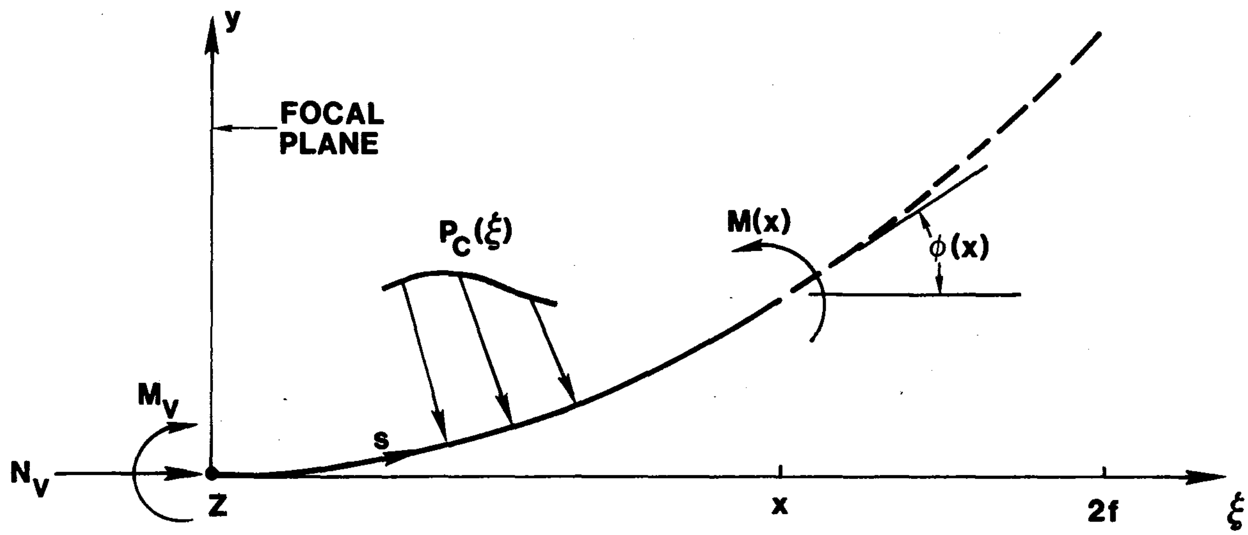

FIGURE 3. Definition of the dummy variable, ξ, local moment, M(x) and slope, ϕ.

desired shape are large. Therefore, the square of (dy/dx) in (3) cannot be ignored in comparison to unity, and it is retained in the calculations. The vertex moment reaction, M_V and the residual moment, M_R, can be found directly from (2) since the curvature of the ideal parabola is known everywhere. In dimensionless form they are

$$\frac{M_V f}{D} = \frac{1}{2} \quad , \tag{4}$$

$$\frac{M_R f}{D} = \frac{\sqrt{2}}{8} \quad . \tag{5}$$

The residual shear, Q_R, can be found from the relation

$$Q_R = -\frac{dM(2f)}{ds} \quad . \tag{6}$$

Using (1),(2) and (3) in (6) gives

$$\frac{Q_R f^2}{D} = \frac{3}{32} \quad . \tag{7}$$

The total moment at any transverse location, x, is found from the equation for moment equilibrium

$$M(x) = \int_0^x dM_p(\xi) - N_V y(x) + M_V \quad , \tag{8}$$

where the incremental moment is given by

$$dM_p(\xi) = - P_C(\xi)(x-\xi)d\xi - P_C(\xi)[y(x)-y(\xi)]dy \quad .$$

The form of $P_C(x)$ is determined to within a single integration constant, C, by solving (2). This constant, and the unknown reaction, N_V, are obtained by satisfying equilibrium of forces in the y and x directions, respectively. Sandia's interests lie with 90° rim angle parabolas [4], or, for those with a full aperture equal to 4f, thus establishing integration limits in the equations for equilibrium in the y and x directions, given by

$$Q_R \cos[\phi(2f)] = \int_0^{2f} P_C(x)dx \quad , \tag{9}$$

$$N_V = -\int_0^{2f} P_C(x)dy + Q_R \sin[\phi(2f)] \quad . \tag{10}$$

A complete solution to the problem is obtained as follows. Using (1) and substituting (8) into (2) gives

$$D \frac{d\phi}{ds} = -\int_0^x P_C(\xi)[(x-\xi) + \frac{\xi}{8f^2}(x^2 - \xi^2)]d\xi - N_V \frac{x^2}{4f} + M_V \quad . \tag{11}$$

An inspection of (11) reveals that, by differentiating the right hand side three times with respect to x, N_V and M_V can be eliminated, leaving an equation in $P_C(x)$ only. Upon using Leibnitz's rule [5] for differentiating an integral with variable limits, three times successively, (11) becomes

$$D \frac{d^4\phi}{dx^3 ds} = -\left[1 + \left(\frac{x}{2f}\right)^2\right]\frac{dP_C(x)}{dx} - \frac{3x}{4f^2} P_C(x) \quad . \tag{12}$$

The left hand side of (12) can be found from knowledge of the desired parabolic shape, given by (1). Substituting (1) into (3) and differentiating three times with respect to x gives for the left hand side of (12),

$$D\frac{d^4\phi}{dx^3 ds} = \frac{15xD}{32f^5}\left[1 + \left(\frac{x}{2f}\right)^2\right]^{-7/2}\left\{3 - 7\left(\frac{x}{2f}\right)^2\left[1 + \left(\frac{x}{2f}\right)^2\right]^{-1}\right\}. \tag{13}$$

It is convenient to introduce the dimensionless variables

$$\eta = \frac{x}{2f} \text{ and } \Psi = \frac{P_C f^3}{D} . \quad (14)$$

The rim of the parabola rim is then located at η=1. Using (14), (13) is substituted into (12) to give

$$\frac{d\Psi}{d\eta} + \frac{3\eta}{(1+\eta^2)} \Psi = - \frac{15\eta}{8(1+\eta^2)^{9/2}} \left[3 - \frac{7\eta^2}{(1+\eta^2)}\right] . \quad (15)$$

Equation (15) is a linear, first order differential equation with a well known general solution [6], which, in the present notation, is

$$\Psi = \frac{-1}{(1+\eta^2)^{3/2}} \left\{\frac{15}{16(1+\eta^2)^2} \left[2 - \frac{7}{3(1+\eta^2)}\right] + C \right\} . \quad (16)$$

The integration constant, C, is found by satisfying vertical equilibrium, (9), the result being

$$C = - \frac{1}{128} .$$

Therefore, (16) becomes

$$\Psi = - \frac{5}{16(1+\eta^2)^{3/2}} \left\{\frac{1}{(1+\eta^2)^2} \left[6 - \frac{7}{(1+\eta^2)}\right] - \frac{1}{40}\right\} . \quad (17)$$

The solution is completed by using (7), (14) and (17) in (10) to obtain the membrane reaction at the vertex, which is, again in dimensionless form,

$$\frac{N_V f^2}{D} = \frac{7}{64} . \quad (18)$$

Use of the inextensional theory, defined by (2), in the presence of a membrane force, N_V, is justified by recognizing that N_V is sufficiently small so that resulting extensions do not effect either equilibrium or the moment - curvature relationships. It must be remembered that the stresses of interest are the contact stresses, σ_C, in the adhesive applied to the backside of the deformed, reflective surface. These stresses are the negative of the contact pressures applied to the front side to deform the initially flat panel. Therefore, $\sigma_C(x) = -P_C(x)$. Figure 4 illustrates, in dimensionless form, how these stresses vary with the projected distance from vertex to edge. It is seen that the tensile stress has a maximum value at the vertex, decreases to zero at a location approximately 1/3 the distance to the edge and remains compressive from there to the edge. The maximum compressive stress occurs approximately 2/3 of the way from vertex to edge. Sandia's interests are with parabolic collectors with f = 0.5 meters, and with mirrored glass reflective panels where $h \simeq 1.27$ mm. Using the results in Fig. 4, these parameters yield a maximum tensile stress at the vertex of approximately 27.6 Pa, a trivial value even for the weakest adhesives. Of course this value will increase with $(h/f)^3$ for other geometries, but, for those of interest here, the more significant contact stress problem will be found in the edge effect zone.

LOSS OF THE TRUE SHAPE - THE EDGE EFFECT PROBLEM

Recall that the above derivation of the adhesive stresses, $\sigma_C(x)$, requires the application of a residual bending moment, M_R, and a residual shear force, Q_R, along the rim of the parabola in order to maintain the nonzero curvature and true shape at the rim. However, these loads are not present in the actual collector. As a result, a loss in the parabolic shape (and thus a loss in optical quality) occurs in a region near

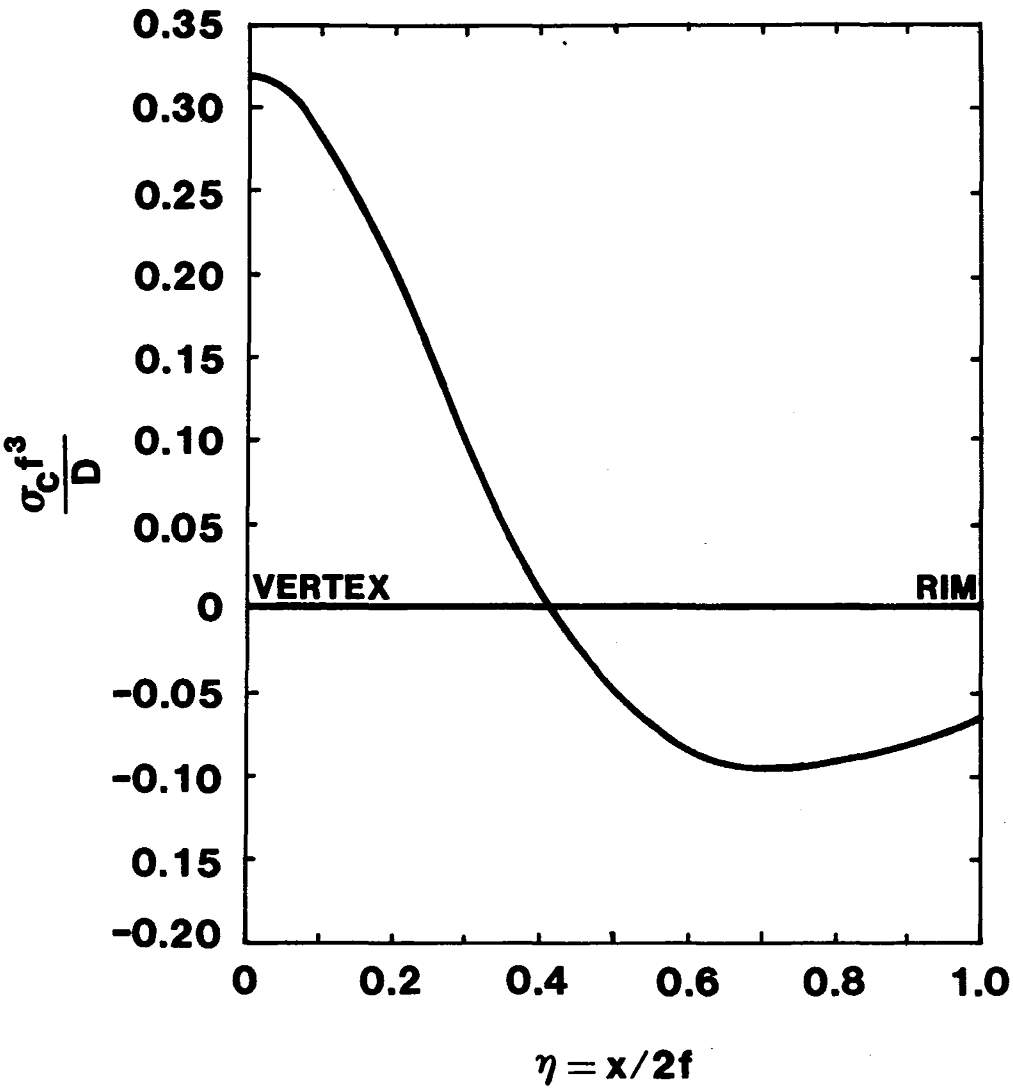

FIGURE 4. Dimensionless contact stresses in adhesive applied to backside of reflective surface after forming.

the rim of the parabola where the curvature tends to zero. Here, a method is proposed to characterize this behavior by treating the region near the rim of the parabola as a flat, semi-infinite plate on an elastic foundation, Fig. 5. Loads equal in magnitude and opposite in direction to M_R and Q_R are applied along the edge of this plate. The normal stresses, σ_R, applied to the plate by the the deformed foundation are calculated and the solution is superimposed on the previous solution, σ_C, to obtain results for the actual zero bending moment and zero shear force edge conditions.

Justification for characterizing the edge region as a flat plate is found in the criterion which stipulates that the radius of curvature be five times the cross section depth [7]. In the present case, the radius of curvature in the region of interest is more than a thousand times the plate thickness so that this criterion is easily met. The semi-infinite characteristic of this model is based on the general theory for the analysis of plates and beams on elastic foundations in which all beams are treated as semi-infinite whose actual lengths, L, satisfy the relationship:

$$L > \frac{3\pi}{2\beta} , \qquad (19)$$

where

$$\beta = \sqrt[4]{\frac{k}{4D}} \quad . \qquad (20)$$

In (19), k is the conventional elastic foundation stiffness [7] and D is the flexural rigidity of the plate. As will be shown later, the values of β corresponding to the parabolic troughs of interest fall between 3.87 and 30.91 mm^{-1}. Thus, if the length of the region being modeled as a flat plate is greater than 122.0 mm then the semi-infinite approximation is valid. Since the region being modeled as a flat plate is greater than 127.0 mm, (19) is satisfied.

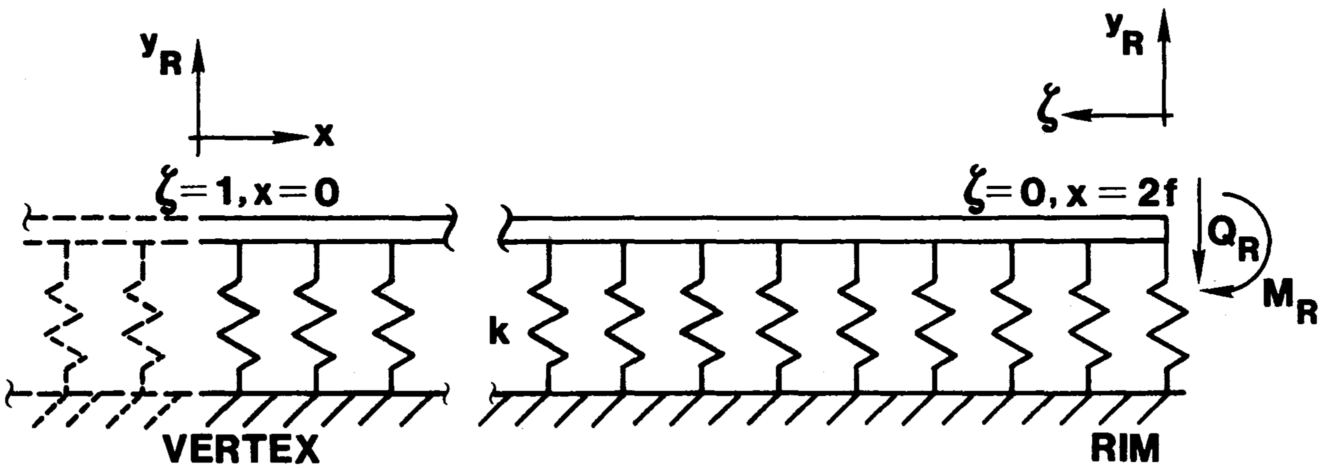

FIGURE 5. Diagram of the flat-plate model of the edge effect region explicating the coordinate system and semi-infinite extension.

Corresponding to the above model are the well known equation and general solution [7]

$$\frac{d^4 w_R}{d\zeta^4} = -\, k w_R \quad , \tag{21}$$

and

$$w_R(\zeta) = e^{-\beta\zeta}[A\cos\beta\zeta + B\sin\beta\zeta] \quad . \tag{22}$$

The solution is subject to the boundary conditions

$$\left.\frac{d^2 w_R}{d\zeta^2}\right|_{\zeta=0} = -\frac{M_R}{D} \quad , \tag{23}$$

$$\left.\frac{d^3 w_R}{d\zeta^3}\right|_{\zeta=0} = -\frac{Q_R}{D} \quad , \tag{24}$$

Using (23) and (24), and transforming to the coordinate defined by

$$x = 2f - \zeta \quad , \tag{25}$$

the solution takes the form

$$w_R(x) = -\frac{e^{-\beta(2f-x)}}{2D\beta^3}\Big[Q_R\cos\beta(2f-x) + \beta M_R\big(\cos\beta(2f-x) - \sin\beta(2f-x)\big)\Big] \quad . \tag{26}$$

The normal stresses in the adhesive, defined by

$$\sigma_R(x) = -kw_R(x) \quad , \tag{27}$$

can be written, using (5), (7) and (26), as

$$\sigma_R(x) = -\frac{\beta^3 D}{16(\beta f)^2} e^{-\beta(2f-x)} \left[\left(3+4\sqrt{2}(\beta f)\right) \cos\beta(2f-x) - 4\sqrt{2}(\beta f)\sin\beta(2f-x)\right] . \tag{28}$$

Another quantity of interest is the surface normal rotation (slope error) defined by

$$w_R'(x) = \frac{dw_R(x)}{dx} \quad . \tag{29}$$

Substituting (26) into (29) gives

$$w_R'(x) = \frac{e^{-\beta(2f-x)}}{64(\beta f)^2} \left[\left(3 + 8\sqrt{2}(\beta f)\right) \cos\beta(2f-x) + 3 \sin\beta(2f-x)\right] . \tag{30}$$

The expression for the normal stress, (28), has the form of a damped, linear oscillator, with maximum compressive stress occuring at the edge where $x = 2f$. Proceeding toward the vertex, the normal stress in the elastic foundation becomes alternately tensile and compressive, rapidly decreasing in peak value. After some preliminary numerical work it was found that the magnitude and location of the maximum stresses were strong functions of β (for fixed f), and unless the stiffness of the elastic foundation, and thus β, was known accurately, large errors in the results could occur. In the case of the parabolic collector, the elastic foundation consists of both the adhesive layer and the substructure itself. Since it is difficult to characterize the local foundation stiffness of the substructure near its rim, a different approach to the numerical evaluation of (28) is taken. Using a laser ray trace procedure [8], and a cursory visual observation, it has been determined that the optical inaccuracies attributed to the edge effect occur within a five to ten centimeter region near the rim of the parabola. According to (26) and (28), the curves for displacement and stress pass through zero whenever

$$\beta - \beta \tan\beta(2f-x) + \frac{3\sqrt{2}}{8f} = 0 \quad . \tag{31}$$

For parabolas of interest here, the quantity $3\sqrt{2}/8f$ can be neglected in comparison to β, as a first approximation, so that (31) is satisfied whenever

$$\beta(2f-x_i) \simeq \frac{n\pi}{4} \; , \; n=1, 5, 9, \ldots \tag{32}$$

where x_i is the location of the ith zero displacement or stress, counting in from the free edge. It can be shown that after the second cross-over from the free edge, stress amplitudes are very small in comparison to those nearer the edge. With this observation, it is assumed that the noticeable edge effects occur between the free edge of the parabola and the second cross-over. By letting δ_2 be the distance from the free edge to the second cross-over, and recognizing that $x_2=2f-\delta_2$, (32) can be used to express the foundation stiffness parameter β in terms of the observed edge effect, or second cross-over distance, δ_2. The result is

$$\beta = \frac{5\pi}{4\delta_2} \quad . \tag{33}$$

Consequently, instead of needing accurate information about the foundation stiffness near the parabolic edge, only the size of the edge effect region need be known. Typical values of β and

δ_2 are shown in Table 1 along with the corresponding stiffness, k, of the foundation representing the adhesive and steel substructure, computed from (20). A glass plate of thickness h = 1.27 mm, Young's modulus E = 70 GPa and Poisson's ration ν = 0.24 (yielding a stiffness D = 12.5 N-m) was used in the calculation of k.

Table 1
Edge Effect Parameters

δ_2(m)	0.01270	0.0254	0.0508	0.0762	0.1016
$\beta(m^{-1})$	308.4	154.6	77.3	51.5	38.6
k(N-m)	1.900×10^5	1.188×10^5	7.426×10^2	1.467×10^2	4.639×10^1

DISCUSSION OF RESULTS

It was pointed out above that for materials used in current constructions, the magnitudes of σ_C are very small suggesting that very little pressure is needed to form the glass panel into the parabolic shape to mate with the substructure. However, in the edge effect regions near the rim additional considerations must be made. In Fig. 6 and 7 the distribution of stress and slope error near the rim resulting from the edge effect have been plotted. Unlike Fig. 4 the actual stresses, σ_R, have been plotted as a function of the actual distance along the parabola because it is impossible to place (28) in a form such as (17) where the left hand side is dimensionless and, moreover, contains quantities which do not depend on the

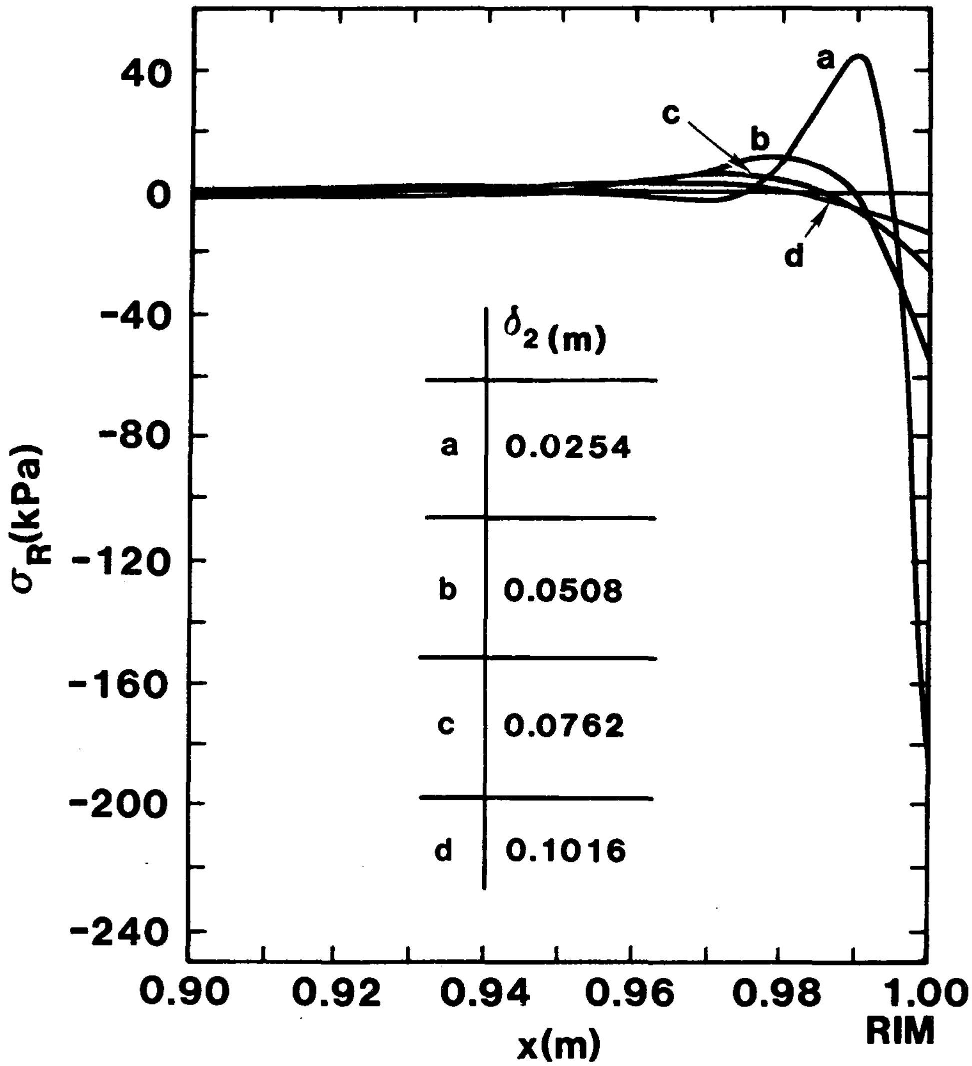

FIGURE 6. Contact stresses in adhesive applied to backside of deformed reflective surface arising from edge effect.

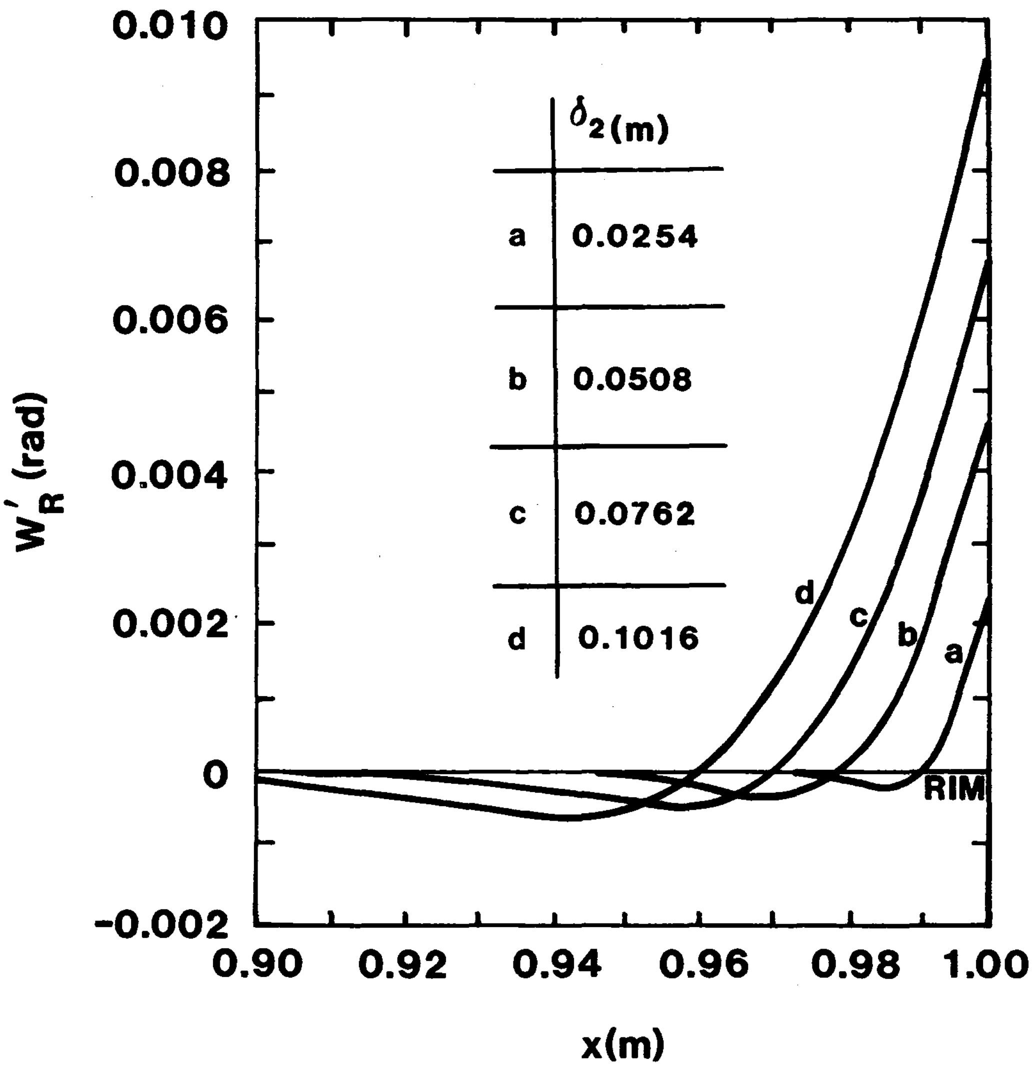

FIGURE 7. Rotation of surface normals (slope error) arising from edge effect.

parameters appearing on the right hand side. In particular, the quantity D in $\sigma_R(x)f^3/D$ is not independent of the parameter β as indicated by equation (20). As a result, the curves have been generated for a variety of sizes of the edge effect region, δ_2.

In examining these figures three observations are of interest: (1) The magnitudes of the stress, σ_R, are an order of magnitude larger than the stresses, σ_C. Thus, while only small pressures are needed to mate the glass panel to the substructure, much higher pressures are needed in order to increase the optical quality near the rim. Theoretically, it would require the residual moment, M_R, to give the correct curvature near the rim. Since this is not possible, some other means (such as the use of clamps) should be considered to make sure the region near the rim is well bonded to the substructure in order to support the higher stresses and minimize the slope errors that result from the edge effect; (2) There is a trade off between the slope error and the adhesive stress. For small values of the second cross-over distance, δ_2, the slope errors are small, but, the stresses in the edge effect region are high. Conversely, for larger values of the second cross-over distance the stresses decrease but the slope errors increase. Since, in either case, the maximum tensile stresses in the adhesive are within acceptable limits, it seems that reducing the size of the affected region and thus reducing the magnitudes of the slope errors is desirable. This is achieved by increasing substructure stiffness, k; (3) The magnitudes of the slope errors predicted in Fig. 6 and 7 correspond well to observed data, Fig. 8. Thus, the model presented in this study should provide a means for optimizing material parameters to increase the optical accuracy and/or decrease the cost of the parabolic design.

The results of this study correspond to the single panel parabolic solar trough design (continuous rim-to-rim reflective surface). Also receiving considerable attention is a double panel design where the full parabola is separated into equal

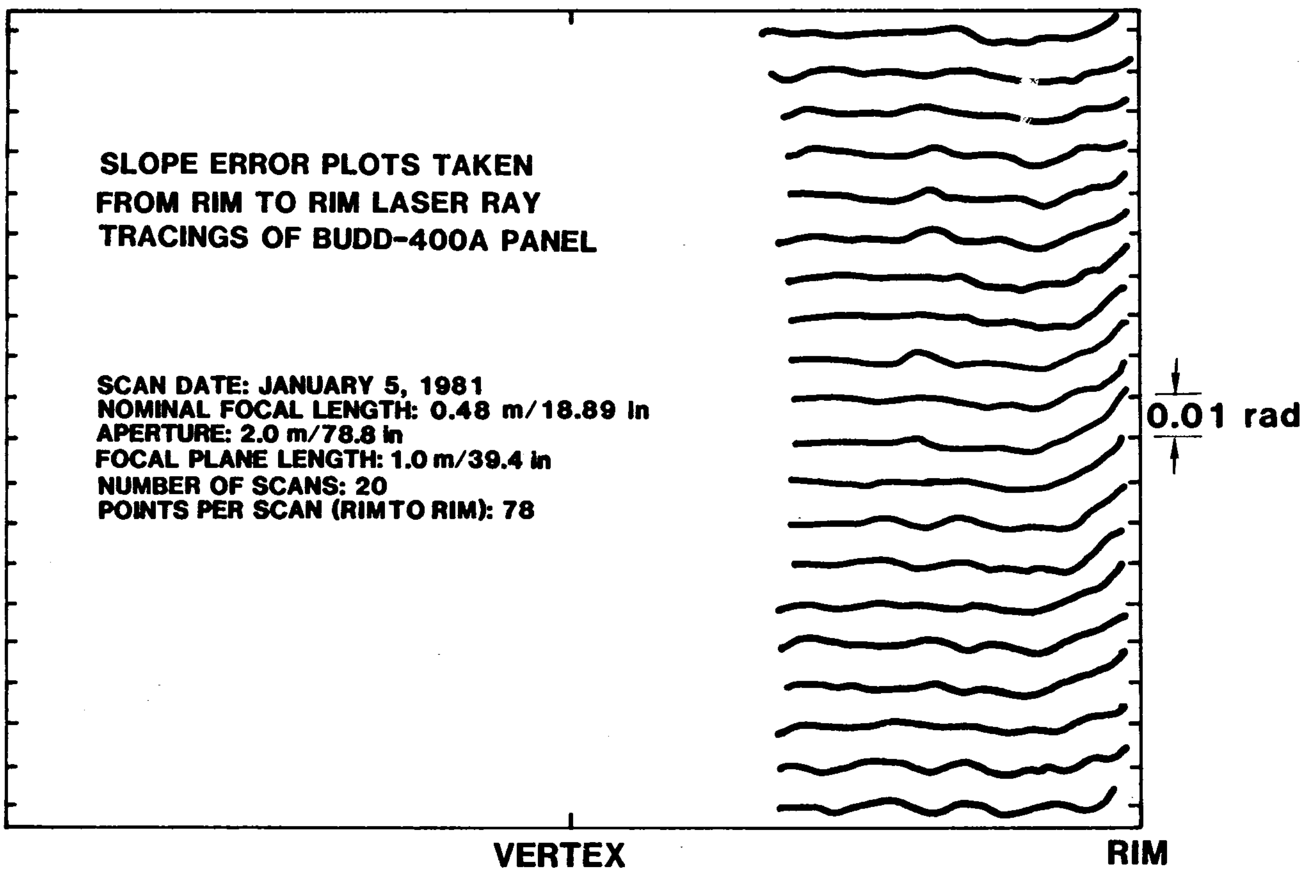

FIGURE 8. Typical results from laser ray tracing showing slope errors at rim.

halves at the vertex. In a continuation of this study the above analysis is repeated for the half parabola and extended to include the behavior of the edge effects which now also appear at the free edges at the vertex. These studies neglect specific substructure design features and involvement. A part of this involvement concerns the effects of gaps in the adhesive (resulting from stamping operations designed to provide stiffness of the substructure through ribbing) on the stress distribution and slope errors near the free edge of the parabola and half-parabola. This problem also is being considered.

SUMMARY

A thin plate (the reflective surface of a parabolic trough collector) can be elastically formed through large displacements to a true parabolic surface by application of a spacially varying surface pressure and uniform bending moments and shear forces applied to a pair of opposing edges. Once formed, the parabolic surface can be bonded to a (comparatively) rigid substructure and expected to retain its shape by virtue of contact stresses developed in the adhesive behind the deformed plate (these stresses are equal in magnitude and opposite in sense to the forming pressures). In most collector designs, provisions are not made for applying the edge loads (moment and shear) necessary to achieve the true parabolic shape. Consequently, optical quality near the collector's rims is reduced and high contact stresses develop in these regions.

The present work includes the derivation of equations necessary to calculate the magnitude of all loads (and stresses) required to mechanically form and hold a true parabolic shape for thin, reflective surfaces, and to calculate local stress variations resulting from necessary boundary (rim) conditions not being satisfied in practice. Considerable

knowledge has been gained with regard to understanding the significance of the edge effect problem, the identity of important parameters involved and how to reduce undesirable consequences in the edge effect zone. Basically, results show that contact stresses over the back surface of the reflective surface due to mechanical forming are relatively small for the materials and geometries of interest here. Additionally, the size of the edge effect zone at the rim(s) of the parabola can be reduced by increasing local foundation stiffness, which also reduces the magnitude of the slope errors there and increases normal stress levels to possibly significant levels.

REFERENCES

1. Bisshopp, K. E. and Drucker, D., "Large Deflection of Cantilevered Beams," Q. Appl. Math., Vol. 3, p. 272 (1945).

2. Fung, Y. C. and Wittrick, W. H., "A Boundary Layer Phenomenon in the Large Deflexion of Thin Plates," Q. J. Mech. and Appl. Math, Vol. 8, Pt. 2, p. 191 (1955).

3. Ashwell, D. G., "The Anticlastic Curvature of Rectangular Beams and Plates," J. Royal Aero. Soc., Vol. 54, p. 708 (1950).

4. Treadwell, G. W., "Design Considerations for Parabolic-Cylindrical Solar Collectors," Proceedings, Intern. Solar Eng. Soc., Vol. 2, p. 235, Winnipeg, Canada (August 1976).

5. Kaplan, W., Advanced Calculus, Addison-Wesley Publishing Col., Inc., Reading, MA (1959).

6. Kreyszig, E., Advanced Engineering Mathematics, John Wiley and Sons, Inc., NY, NY (1963).

7. Boresi, A. P.; Sidebottom, O. M.; Seely, F. B and Smith J. O., Advanced Mechanics of Materials, 3rd Edition, John Wiley and Sons, Inc., NY, NY (1978).

8. Hansche, B. D., "Laser Ray Trace Tester for Parabolic Trough Solar Collectors," Instrum. Soc. of Am. Proceedings, Vol. 19, No. 2, p. 43 (1980).

Distribution to:
AAI Corporation
P. O. Box 6787
Baltimore, MD 21204

Acurex Aerotherm
485 Clyde Avenue
Mountain View, CA 94042
Attn: J. Vindum

Alpha Solarco
1014 Vine Street
Suite 2230
Cincinnati, OH 45202

Argonne National Laboratory (3)
9700 South Class Avenue
Argonne, IL 60439
Attn: K. Reed
W. W. Schertz
R. Winston

BDM Corporation
1801 Randolf Street
Albuquerque, NM 87106
Attn: T. Reynolds

Black and Veatch (2)
P. O. Box 8405
Kansas City, MO 64114
Attn: Dr. J. C. Grosskreutz
D. C. Gray

Budd Company (2)
Fort Washington, PA 19034
Attn: W. W. Dickhart
W. Eggert

Custom Engineering, Inc.
2805 South Tejon St.
Englewood, CO 80110
Attn: C. A. de Moraes

Del Manufacturing Co.
905 Monterey Pass Road
Monterey Park, CA 91754
Attn: M. M. Delgado

Donnelly Mirrors, Inc.
49 West Third Street
Holland, MI 49423
Attn: J. A. Knister

E-Systems, Inc.
Energy Tech. Center
P. O. Box 226118
Dallas, TX 75266
Attn: R. R. Walters

Edison Electric Institute
90 Park Avenue
New York, NY 10016
Attn: L. O. Elsaesser

Electric Power Research Institute (2)
3412 Hillview Avenue
Palo Alto, CA 94303
Attn: Dr. J. Cummings
J. E. Bigger

Florida Solar Energy Center (2)
300 State Road, Suite 401
Cape Canaveral, FL 32920
Attn: C. Beech
D. Block

General Atomic
P. O. Box 81608
San Diego, CA 92138
Attn: A. Schwartz

General Electric Co. (2)
P. O. Box 8661
Philadelphia, PA 19101
Attn: W. Pijawka
C. Billingsley

General Motors Corporation
Technical Center
Warren, MI 48090
Attn: J. F. Britt

Georgia Institute of Technology
Atlanta, GA 30332
Attn: J. D. Walton

Haveg Industries, Inc.
1287 E. Imperial Highway
Santa Fe, Springs, CA 90670
Attn: J. Flynt

Hexcel
11711 Dublin Blvd.
Dublin, CA 94566
Attn: R. Johnston

Honeywell, Inc.
Energy Resources Center
2600 Ridgeway Parkway
Minneapolis, MN 55413
Attn: J. R. Williams

Jacobs Engineering Co.
251 South Lake Avenue
Pasadena, CA 91101
Attn: R. Morton

Jet Propulsion Laboratory (3)
4800 Oak Grove Drive
Pasadena, CA 91103
Attn: J. Becker
J. Lucas

Los Alamos Scientific Lab. (3)
Los Alamos, NM 87545
Attn: J. D. Balcomb
C. D. Bankston
D. P. Grimmer

McDonnell-Douglas Astronautics Company (3)
5301 Bolsa Avenue
Huntington Beach, CA 92647
Attn: J. B. Blackmon
J. Rogan
D. Steinmeyer

New Mexico State University
Solar Energy Department
Las Cruces, NM 88001

Office of Technology Assessment
U. S. Congress
Washington, DC 20510
Attn: R. Rowberg

Owens-Illnois
1020 N. Westwood
Toledo, OH 43614
Attn: Y. K. Pei

PPG Industries, Inc.
One Gateway Center
Pittsburg, PA 15222
Attn: C. R. Frownfelter

PRC Energy Analysis Company
7600 Old Springhouse Road
McLean, VA 22101

Parsons of California
3437 S. Airport Way
Stockton, CA 95206
Attn: D. R. Biddle

Schott America
11 East 26th St.
New York, NY 10010
Attn: J. Schrauth

Solar Energy Information Center
1536 Cole Blvd.
Golden, CO 80401
Attn: R. Ortiz

Solar Energy Research Institute (13)
1536 Cole Blvd.
Golden, CO 80401
Attn: B. L. Butler
L. G. Dunham (4)
B. P. Gupta
F. Kreith
J. Thornton
K. Touryan
N. Woodley
D. W. Kearney
C. Bishop
B. Feasby
M. Murphy

Solar Kinetics, Inc.
P. O. Box 47045
8120 Chancellor Row
Dallas, TX 75247
Attn: G. Hutchison

Southwest Research Institute
P. O. Box 28510
San Antonio, TX 78284
Attn: D. M. Deffenbaugh

W. B. Stine
317 Monterey Rd., Apt. 22
South Pasadena, CA 91303

Suntec Systems, Inc.
2101 Wooddale Drive
St. Paul, MN 55110
Attn: L. W. Rees

U. S. Department of Energy (3)
Albuqueque Operations Office
P. O. Box 5400
Albuquerque, NM 87185
Attn: G. N. Pappas
C. B. Quinn
J. Weisiger

U. S. Department of Energy
Division of Energy Storage
Systems
Washington, DC 20545
Attn: J. Gahimer

U. S. Department of Energy (8)
Division of Solar Thermal
Energy Systems
Washington, DC 20545
Attn: W. W. Auer
G. W. Braun
J. E. Greyerbiehl
W. Hocheiser
J. E. Rannels
F. Wilkins
D. Stogowski

U. S. Department of Energy (2)
San Francisco Operations Office
1333 Broadway, Wells Fargo Bldg.
Oakland, CA 94612
Attn: R. W. Hughey

University of New Mexico (2)
Department of Mechanical Eng.
Albuquerque, NM 87113
Attn: M. W. Wilden
W. A. Cross

Viking
3467 Ocean View Blvd.
Glendale, CA 91208
Attn: G. Guranson

2540 K. L. Gillespie
2541 C. M. Gabriel
2542 R. S. Pinkham
3141 T. L. Werner (5)
3161 J. E. Mitchell
4000 A. Narath
4700 J. H. Scott
4710 G. E. Brandvold
4715 R. H. Braasch
4716 J. F. Banas (100)
4717 J. A. Leonard
4720 D. G. Schueler
4750 V. L. Dugan
5000 J. K. Galt
5500 O. E. Jones
5510 D. B. Hayes
5513 D. W. Larson
5520 T. B. Lane
5522 T. G. Priddy
5522 R. K. Wilson (15)
5523 R. C. Reuter, Jr. (15)
5523 D. B. Clauss
5523 J. R. Koteras
5523 B. A. Lewis
5530 W. Herrmann
5814 F. P. Gerstle, Jr.
6011 Patents
8120 W. E. Alzheimer
8123 D. J. Bammann
8266 E. A. Aas (2)
8450 C. Selvage
8450 R. C. Wayne
3151 W. L. Garner (3)
(Unlimited Release)
For DOE/TIC
(Unlimited Release)

☆ U.S. GOVERNMENT PRINTING OFFICE: 1981-0-576-021/649